Materials Today Bio 32 (2025) 101795

Contents lists available at ScienceDirect

Materials Today Bio

journal homepage: www.journals.elsevier.com/materials-today-bio

Berberine hydrochloride-loaded liposomes-in-hydrogel microneedles achieve the efficient treatment for psoriasis

Si Shen, Wang Shen [1], Lu Wang [1], Bin Sun, Yongli Zhang, Yong Zhang, Ruoyang Jia, Yang Wu, Xue Chen, Keang Cao, Yuqing Fang, Hongmei Xia [*]

College of Pharmacy, Anhui University of Chinese Medicine, No. 350, Long Zi Hu Road, Hefei, 230012, China

ARTICLE INFO

Keywords:
Psoriasis
Hydrogel microneedles
Antioxidant
Liposomes
Inflammatory skin diseases

ABSTRACT

Psoriasis is a common immune-mediated squamous skin disease, primarily characterized by the over proliferation of keratinocytes and a significant thickening of the stratum corneum. Traditional systemic drug delivery therapies often fall short due to low drug bioavailability and significant toxic side effects. Topical medications, while capable of achieving local or systemic treatment via transdermal routes, face limitations in psoriasis patients due to the abnormal thickening of the epidermis, which reduces skin permeability and hampers drug penetration efficiency. Hydrogel microneedles, as an emerging transdermal drug delivery technology, offer significant advantages such as high permeability, ease of use, low toxicity and side effects, and controlled release. Therefore, this study developed a liposome-hydrogel microneedle delivery system for the administration of berberine hydrochloride. We successfully prepared berberine hydrochloride-loaded liposomes (Ber-LPs) with high encapsulation efficiency and good stability, and integrated them into hydrogel microneedles crosslinked with PVA and PEGDA (Ber-LPs-PEGDA&PVA MNs) through a photocuring method. These microneedles exhibit an intact structure, high mechanical strength, and effective skin penetration. In vivo studies on anti-psoriatic effects showed that, compared to the model group, Ber-LPs-PEGDA&PVA MNs significantly alleviated imiquimod-induced psoriasis-like symptoms in mice, reduced skin epidermal thickness, decreased the expression levels of inflammatory cytokines, and lowered the expression of CD31 and VEGF, demonstrating excellent therapeutic efficacy. Additionally, the microneedles exhibited good drug release properties, antioxidant capacity, and biocompatibility. The novel hydrogel microneedle drug delivery system developed in this study offers a safe and effective solution for the treatment of psoriasis, with significant potential for clinical application.

1. Introduction

Psoriasis is a T-cell-mediated dermatological condition primarily characterized by erythema and scales. Epidemiological surveys indicate that approximately 125 million individuals worldwide are affected by this disease [1]. Psoriasis is often accompanied by severe itching and a high recurrence rate, with prolonged treatment cycles that significantly impair patients' quality of life and impose substantial psychological, physiological, and economic burdens [2]. The main pathological manifestations of psoriasis include hyperkeratosis with parakeratosis, thinning of the stratum spinosum above the dermal papillae, dilatation of dermal papillary capillaries, and pronounced infiltration of inflammatory cells [3]. Among these, abnormalities in skin vascular distribution and formation in lesional areas typically emerge earliest, manifesting as extensive vascular dilation, tortuosity, and increased permeability [4]. Angiogenesis is triggered by angiogenic factors, with vascular endothelial growth factor (VEGF) being the most potent. VEGF activates endothelial cells, promoting their proliferation and migration to perivascular regions, thereby forming numerous vascular structures that drive epidermal hyperplasia in psoriasis [5]. Although the precise etiology and pathogenesis of psoriasis remain incompletely understood, most studies suggest that inflammatory cytokines such as tumor necrosis factor-α (TNF-α), interleukin-17 (IL-17), interferon-γ (IFN-γ), IL-23, and VEGF interact in a network to drive disease progression [6–8]. Current treatments for psoriasis primarily include topical agents, phototherapy, and systemic therapies [9]. Traditional systemic drug delivery methods suffer from low bioavailability and toxic side effects, leading to suboptimal therapeutic outcomes [10]. Topical agents achieve systemic or

* Corresponding author.
E-mail address: sm_shine@ahtcm.edu.cn (H. Xia).
[1] These authors should be co-first authors because of their contributed equally to this work.

https://doi.org/10.1016/j.mtbio.2025.101795
Received 7 February 2025; Received in revised form 13 April 2025; Accepted 22 April 2025
Available online 25 April 2025

local treatment via transdermal routes, but the thickened epidermis and reduced skin permeability in psoriasis patients result in insufficient drug penetration [11]. Therefore, designing drug delivery systems capable of overcoming the skin barrier and enhancing drug utilization is crucial for psoriasis management.

The rapid advancement of nanotechnology has opened up new avenues for enhancing targeted delivery, improving skin penetration, and elevating treatment efficacy and safety [12]. Drugs encapsulated within lipid-based nanocarriers can effectively permeate the stratum corneum due to their lipophilic nature [13]. These nanocarriers also offer advantages such as high encapsulation efficiency, high stability, and sustained drug release. Liposomes represent a promising and significant class of drug delivery vehicles [14]. Currently, numerous liposomal formulations have been employed in the treatment of skin diseases [15,16]. Furthermore, liposomes can enhance drug stability and solubility, thereby improving the bioavailability of poorly soluble drugs.

Berberine hydrochloride (Ber), also known as berberine, is an isoquinoline alkaloid [17] and the primary active compound in *Coptis chinensis* (commonly known as Huanglian in Chinese medicine). It is primarily used to treat intestinal infections, including acute gastroenteritis and bacterial dysentery [18]. Pharmacological studies have also demonstrated that Ber possesses antibacterial, antiviral, and anti-inflammatory properties [19]. Ber can inhibit inflammatory cell infiltration and suppress the production of TNF-α, IL-23, and IFN-γ through multiple pathways, thereby exerting therapeutic effects in various diseases [20–22]. Additionally, Ber effectively scavenges reactive oxygen species and various free radicals while attenuating lipid peroxidation reactions [23]. With the advancement of medicinal chemistry research, berberine hydrochloride has exhibited additional pharmacological effects. In recent years, it has been found to have certain therapeutic effects in treating various skin disorders [24]. However, the widespread use of berberine hydrochloride is limited by its low bioavailability [25]. By employing a novel nano-liposomal drug delivery system, encapsulating berberine hydrochloride within nano-liposomes significantly enhances its bioavailability and stability. Nevertheless, achieving ideal transdermal drug delivery efficiency necessitates the administration of substantial amounts of the drug.

Microneedles, as a typical transdermal medical device, can penetrate the stratum corneum with their micrometer-scale tips, creating microchannels that significantly enhance drug delivery efficiency. Consequently, they hold promising application prospects in the field of biomedical engineering [26–28]. Unlike solid microneedles and dissolving microneedles, hydrogel microneedles absorb tissue fluid upon insertion into the subcutaneous layer, causing swelling without dissolution. The drugs loaded within the hydrogel microneedles can then be precisely delivered to the subcutaneous tissue through the network formed by swelling, relying on concentration gradients [29–31]. Compared to dissolvable microneedles, hydrogel microneedles can carry drugs in the base region, substantially increasing the drug loading capacity [32]. Moreover, the preparation process of hydrogel microneedles is more straightforward and rapid than that of solid microneedles, with lower production costs [33,34]. Hydrogel microneedles not only enhance drug loading capacity but also enable controlled drug release through the regulation of cross-linked networks [35].

Therefore, this study designed a novel hydrogel microneedle for the delivery of small molecule drugs. By delivering nanomedicines from the epidermis to the dermal layer, the drug permeation efficiency and utilization rate were significantly improved. In this research, a novel drug delivery system, namely hydrogel microneedles loaded with berberine hydrochloride liposomes (Ber-LPs-PEGDA&PVA MNs), was successfully developed. Specifically, hydrogel microneedles cross-linked with polyvinyl alcohol (PVA) and poly(ethylene glycol) diacrylate (PEGDA) were fabricated via photopolymerization, and then loaded with Ber-LPs nanoparticles. The morphology, mechanical properties, insertion ability, antioxidant performance, biocompatibility, and in vitro transdermal release properties of Ber-LPs-PEGDA&PVA MNs were evaluated. The therapeutic effects of Ber-LPs-PEGDA&PVA MNs on an imiquimod-induced mouse model of psoriasis were investigated. The impacts of Ber-LPs-PEGDA&PVA MNs on epidermal thickness, inflammatory cell infiltration, levels of inflammatory cytokines, levels of oxidative stress factors, and the expression of angiogenesis-related proteins in mice were observed. All the aforementioned results indicated that Ber-LPs-PEGDA&PVA MNs could significantly alleviate psoriasis-like symptoms in mice, and the therapeutic effect was superior to other treatment groups. Compared with traditional treatment methods, Ber-LPs-PEGDA&PVA MNs demonstrated more remarkable therapeutic efficacy. Their unique design of nano-liposomes and hydrogel microneedles not only enhanced the bioavailability and stability of drugs but also overcame the skin barrier, achieving efficient delivery and sustained release of drugs. This study provides a novel strategy for the treatment of psoriasis.

2. Materials and methods

2.1. Materials

Berberine hydrochloride was purchased from Shanxi Zhonghong Biotechnology Co., Ltd. (Shanxi, China). Polyvinyl alcohol (PVA,1778 low-viscosity type), polyethylene glycol diacrylate (PEGDA, average molecular weight 1000), and 2-Hydroxy-4'-(2-hydroxyethoxy)-2-methylpropiophenone (I2959) were provided by Aladdin Biochemical Technology Co., Ltd. (Shanghai, China). Egg yolk phospholipid and cholesterol were obtained from Sinopharm Chemical Reagent Co., Ltd. (Shanghai, China). 1,1-Diphenyl-2-picrylhydrazyl (DPPH) was sourced from Source Leaf Biotechnology Co., Ltd. (Shanghai, China). 2,2′-Azobis (2-methylpropionamidine) dihydrochloride and potassium persulfate were acquired from Macklin Biochemical Technology Co., Ltd. (Shanghai, China). IMQ cream (5 %) was purchased from Sichuan Mingxin Pharmaceutical Co., Ltd. (Sichuan, China). The SOD, CAT, GSH-PX, and MDA kits used in this study were purchased from Nanjing Jiancheng Bioengineering Institute (Nanjing, China). Mouse IL-17, IL-23, TNF-α, and IFN-γ ELISA kits were obtained from Shanghai Weiao Biotechnology Co., Ltd. (Shanghai, China).

2.2. Animals

Male KM mice (6 weeks old; 20 ± 2 g) were purchased from the Experimental Animal Center of Anhui University of Chinese Medicine. All experimental animals were housed under the same environmental and nutritional conditions, with the indoor temperature maintained at (25 ± 2) °C, relative humidity kept between 55 ± 15 %, and a light cycle of 12 h. The housing environment was quiet and well-ventilated, and all experimental animals were provided with regular feed and water, with bedding changed daily.

All animal experiments were conducted in accordance with the guidelines approved by the Ethics Committee of Anhui University of Chinese Medicine, ensuring animal welfare, with the ethics number AHUCM-mouse-2024189.

2.3. Preparation and characterization of Ber-LPs

Berberine Hydrochloride-Loaded Liposomes (Ber-LPs) were prepared using the ethanol injection method [36] (Fig. 1A). Initially, a specific mass ratio of egg yolk phospholipid and cholesterol were completely dispersed in a certain volume of anhydrous ethanol using ultrasound. Next, under magnetic stirring, the resulting organic solution was injected into a phosphate-buffered solution (PBS) containing a specific concentration of Ber using a syringe pump. Hydration was then carried out at 55 °C for 1 h to remove ethanol and part of the water. Finally, the colloidal suspension was filtered across the 0.22 μm filter to obtain a sterile formulation, and the Ber-LPs were prepared and stored at 4 °C.

In the Box-Behnken design method employed by Design-Expert

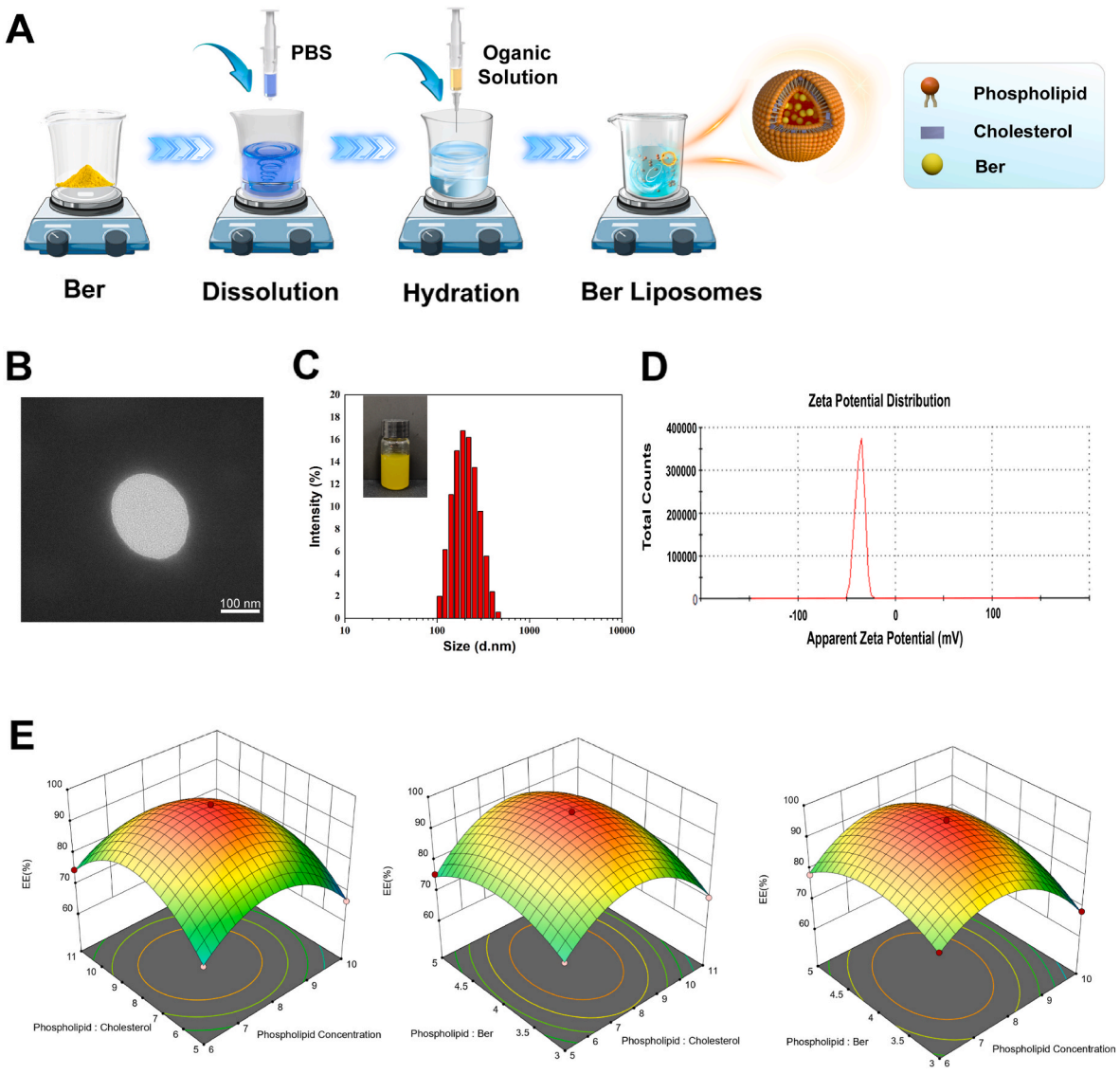

Fig. 1. Preparation and characterization of Ber-LPs. (A) Schematic Diagram of the Preparation Process of Ber-LPs. (B) TEM Image of Ber-LPs. (C) Particle Size Distribution of Ber-LPs. (D) Zeta Potential Graph of Ber-LPs. (E) Response Surface Optimization Design for the Preparation of Ber-LPs.

software (version 13, State-Ease Inc., USA), the encapsulation efficiency (EE%) of Ber-LPs was set as the response value, with phospholipid concentration (6, 8, and 10 mg/mL), ratio of phospholipid-to-cholesterol (5:1, 8:1, and 11 (w:w)), and ratio of phospholipid-to-drug (3:1, 4:1, and 5:1 (w:w)) being selected as the independent variables. Through this process, an optimized formula for Ber-LPs were obtained.

The morphology of the liposomes prepared above were observed using the Hitachi HT7700 Transmission Electron Microscope (TEM) (Tokyo, Japan). Firstly, the liposomes were appropriately diluted with phosphate-buffered solution (PBS), then dropped onto a clean copper grid and allowed to dry. Finally, the dried liposomes solution was negatively stained with 2 % phosphorite acid, and observed after air-drying. Dynamic Light Scattering (DLS) technology (Malvern Instruments, Malvern, UK) was employed to test the particle size, polydispersity index (PDI), and zeta potential of Ber-LPs.

2.4. Preparation and characterization of MNs

The matrix composition significantly influenced the molding performance, mechanical properties, and drug release characteristics of Ber-LPs-PEGDA&PVA MN. A comprehensive evaluation was conducted based on the compatibility of different matrix ratios, the amount of bubbles after resting for 60 min, the ease of demolding, the needle retention rate, and the swelling rate of the microneedles. The matrix with the highest score was selected for further optimization and ultimately determined as the ideal material for fabricating hydrogel microneedles.

Based on the screening results of the matrix materials for Ber-LPs-PEGDA&PVA MNs, Irgacure2959 (I2959) was selected as the UV photoinitiator. The hydrogel microneedles loaded with berberine hydrochloride liposomes (Ber-LPs-PEGDA&PVA MNs) were then fabricated through photopolymerization (Fig. 2A). Firstly, a PEGDA polymer solution was mixed with the I2959 (0.5 % w/w). Then, PEGDA and PVA were blended in the ratio of 10:3 (v/v) to prepare a prepolymer solution, which was further mixed with Ber-LPs in a 10:1 (v/v) ratio. This mixture solution was carefully injected into a polydimethylsiloxane (PDMS) microneedle mold and placed in a vacuum oven preheated to 30 °C. The pressure was reduced to 25 inches of Hg and maintained for 30 min. After the solution entered the needle tips, the vacuum valve was opened, and the mixture was allowed to stand for 60 min to ensure that bubbles fully rose to the liquid surface, burst, and disappeared. Subsequently, crosslinking under UV light (360 nm, 5 W) was performed to form

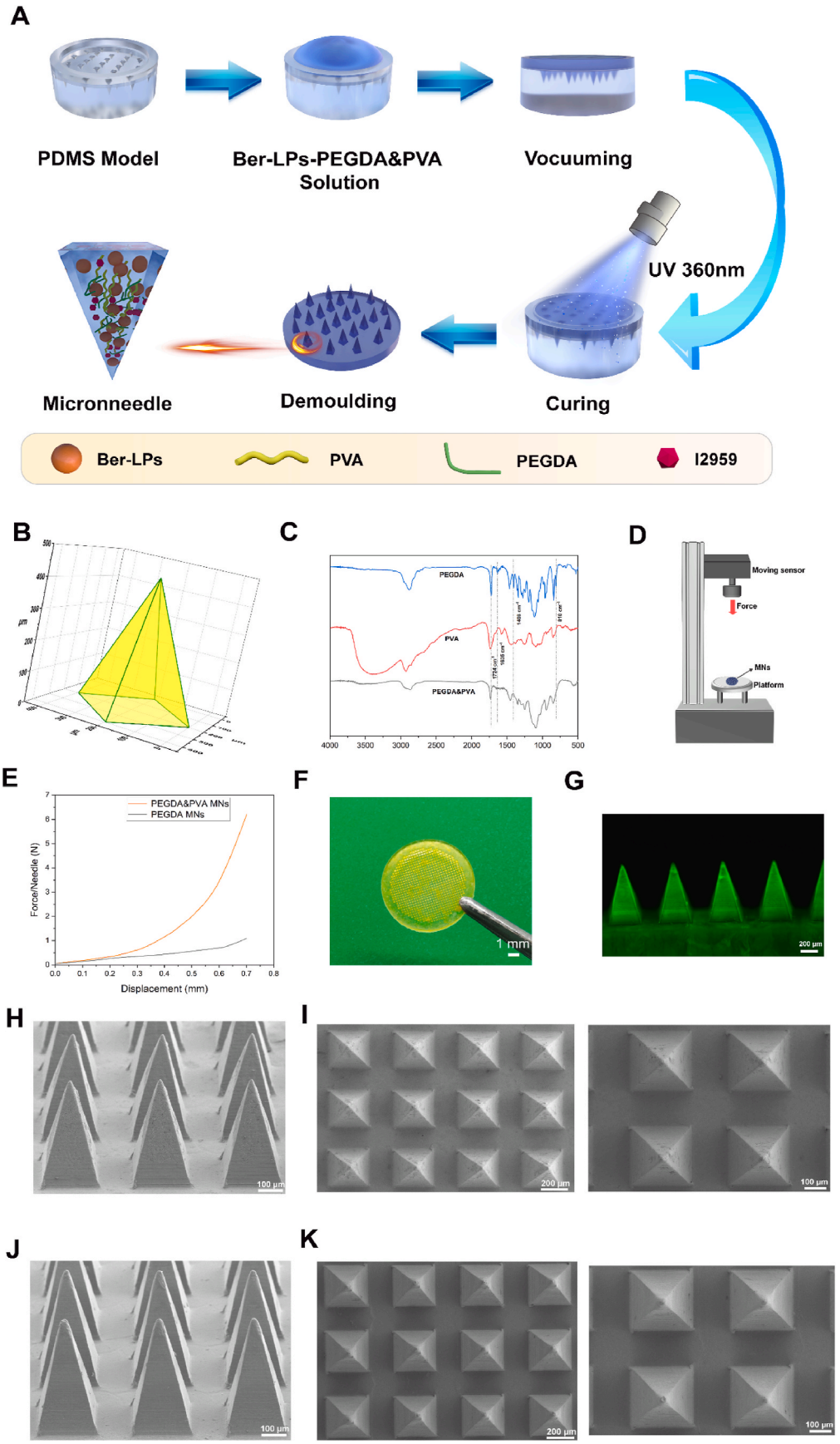

(caption on next page)

Fig. 2. Preparation and characterization of MNs. (A) Schematic diagram for the preparation of Ber-LPs-PEGDA&PVA MNs arrays. (B) The design of MNs body. (C) Infrared spectra of PEGDA, PVA, and PEGDA&PVA. (D) Schematic diagram of the texture analyzer test for the mechanical properties of MNs. (E) Mechanical strength of PEGDA&PVA MNs and PEGDA MNs. (F) Digital camera images of Ber-LPs-PEGDA&PVA MNs. (G) The THUNDER images of Ber-LPs-PEGDA&PVA MNs. (H) SEM side view of PEGDA&PVA MNs. (I) SEM top view of PEGDA&PVA MNs. (J) SEM side view of PEGDA MNs. (K) SEM top view of PEGDA MNs.

microneedles. Finally, the microneedle array was carefully peeled off from the reverse mold and placed in a desiccator overnight to fully crosslink any radicals generated during the irradiation process, yielding Ber-LPs-PEGDA&PVA MNs. A similar procedure was followed to prepare blank PEGDA&PVA MNs without the addition of Ber-LPs. PEGDA MNs which were neither crosslinked with PVA nor supplemented with Ber-LPs, were also prepared using this method.

The chemical compositions of the prepared PEGDA&PVA MNs, PEGDA MNs, and PVA samples were characterized using Fourier Transform Infrared (FTIR) spectroscopy (IRAffinity-1s, Japan). The dried MNs samples were grinded and mixed with dried KBr powder to form pellets. The wavelength range for scanning was from 4000 cm^{-1} to 500 cm^{-1}, and the process was repeated three times to obtain the results.

The mechanical strength of the MNs was analyzed using a texture analyzer (TA.XT, China) of a universal mechanical testing machine. A TA2 probe with a diameter of 2 mm was used to approach the MNs vertically at a speed of 0.02 mm/s. The sensor displacement and the force applied to the MNs were recorded starting from the first contact between the sensor and the tips of the MNs until the tips broke.

To evaluate the uniformity of Ber-LPs dispersion within the MNs, the morphology of the Ber-LPs-PEGDA&PVA MNs was observed using the wide-field THUNDER system (Leica, Italy), leveraging the intrinsic fluorescence of Ber. The morphology of the MNs was characterized using Scanning Electron Microscopy (SEM) (Zeiss Sigma 500, Germany).

2.5. Drug loading capacity of MNs

To assess the drug loading capacity of Ber-LPs-PEGDA&PVA MNs and Ber-LPs-PEGDA MNs, the microneedle arrays were immersed in 50 mL of water. The solution was stirred overnight at 100 r/min, followed by sonication to ensure complete drug release. A 1 mL aliquot of the solution was then mixed with 1 mL of methanol. After sonicating the mixture for 30 min, it was centrifuged at 12000 r/min for 10 min. The supernatant was filtered through a 0.22 μm pore-sized membrane filter. The filtrate was diluted with methanol to an appropriate concentration, and the absorbance was measured at 345 nm to determine the drug content of the microneedles.

2.6. In vitro transdermal release study of MNs

The in vitro transdermal release capability of microneedles was evaluated using a Franz diffusion cell apparatus (Fig. 4A). A PBS buffer solution with pH 7.4 was used as the release medium to evaluate the transdermal release of Ber, Ber-LPs, Ber-LPs-PEGDA&PVA MNs, and Ber-LPs-PEGDA MNs. Mouse excised skin was mounted on the Franz diffusion cell with the stratum corneum facing the donor compartment. Approximately 200 μg of Ber solution, Ber-LPs suspension, Ber-LPs-PEGDA&PVA MNs, and Ber-LPs-PEGDA MNs were placed into the donor compartment, respectively. The collection pool was filled with PBS buffer solution at pH 7.4. The diffusion cell apparatus was placed in a magnetic stirrer at 37 °C with a stirring speed of 100 r/min. At predetermined time intervals (0.5, 1, 2, 4, 6, 8, 10, 12, and 24 h), 2.0 mL of the receiver solution was withdrawn, and an equal volume of fresh PBS solution was added back to maintain sink conditions. The absorbance of the samples was measured at 345 nm, with three replicates for each formulation. The formula for calculating the cumulative amount of transdermal drug per unit area (Q) is as follows:

$$Q = \frac{m_t}{S}$$

where "m_t" represents the cumulative drug release amount at time point t, and "S" represents the drug release area of the diffusion cell. Plot the transdermal release curve with T as the horizontal coordinate and Q as the vertical coordinate, respectively.

2.7. Insertion experiment of Ber-LPs-PEGDA&PVA MNs

Using excised mouse skin as a model, a puncture test was conducted. The Ber-LPs-PEGDA&PVA MNs were pressed and inserted into the mouse skin for 2 min. After removing the microneedle array, the recovery of the puncture holes in the mouse skin was observed, and images were recorded using a Motic stereo microscope. To prepare histological specimens, the insertion site of the microneedles was excised from the skin using a scalpel. The skin samples were then fixed in 4 % paraformaldehyde for 24 h, embedded in paraffin, sectioned using a cryostat, and stained with hematoxylin and eosin (H&E) for examination under an optical microscope.

2.8. Antioxidant capacity of Ber-LPs-PEGDA&PVA MNs

2.8.1. DPPH free radical scavenging ability

1,1-Diphenyl-2-picrylhydrazyl (DPPH), in the presence of radical scavengers, can accept an electron or hydrogen atom to form a stable DPPH-H compound, which causes the solution to decolorize and reduce its absorbance [37]. Therefore, DPPH radicals can be used as an indicator to evaluate the antioxidant performance of antioxidants. In this paper, the DPPH radical scavenging ability of Ber-LPs-PEGDA&PVA MNs was determined based on previously described methods with slight modifications [38]. The MNs extract was prepared by soaking a certain mass of Ber-LPs-PEGDA&PVA MNs in a fixed volume of aqueous solution. Briefly, 1.0 mL of MNs extract of varying concentrations (0.04、0.08、0.12、0.16 mg/mL) was added to 1.0 mL of DPPH solution (0.01 mM) dissolved in absolute ethanol. After being thoroughly mixed and gently shaken, the mixture was incubated in the dark for 30 min. Finally, the absorbance of the sample group at 517 nm was recorded. The absorbance of a mixture of 1 mL of DPPH solution and 1.0 mL of absolute ethanol was set as the blank control group, while the absorbance of a mixture of 1 mL of absolute ethanol and 1 mL of MNs extract was set as the sample control group. The formula for calculating the DPPH radical scavenging activity is as follows:

$$\text{Scavenging rate } (\%) = \left(1 - \frac{A_s - A_c}{A_0}\right) \times 100\%$$

where "A_0" represents the absorbance of the blank control group, "A_s" represents the absorbance of the sample group, and "A_c" represents the absorbance of the sample control group.

2.8.2. ABTS free radical scavenging ability

ABTS must be oxidized by an oxidizing agent, such as potassium persulfate or manganese oxide, to generate the stable blue-green ABTS+· radical [39]. ABTS+· exhibits a maximum absorption peak at 734 nm, with the absorbance being directly proportional to the radical concentration [40]. Compared to the DPPH method, the ABTS method is more sensitive to hydrophilic antioxidants and has a shorter reaction time. An ABTS solution in absolute ethanol (7 mM) was mixed with an equal volume of potassium persulfate (5 mM) and allowed to react in the dark for 12 h. The mixture was then diluted with absolute ethanol to achieve an initial absorbance of 0.70 ± 0.02 at the wavelength of 734 nm. Next, 1.0 mL of MNs extract at different concentrations (0.04、0.08、0.12、0.16 mg/mL) was mixed with 3.0 mL of the diluted ABTS

solution, and the mixture was incubated at room temperature for 10 min. The absorbance of the sample group was then recorded under a wavelength of 734 nm. The absorbance of a mixture of 3.0 mL of ABTS solution and 1.0 mL of absolute ethanol was set as the blank control group, while the absorbance of a mixture of 3.0 mL of absolute ethanol and 1.0 mL of MNs extract was set as the sample control group. The formula for calculating the ABTS radical scavenging activity is as follows:

$$\text{Scavenging rate}\ (\%) = \left(1\text{-}\frac{A_s\text{-}A_c}{A_0}\right) \times 100\%$$

where "A_0″ represents the absorbance of the blank control group, "A_s" represents the absorbance of the sample group, and "A_c" represents the absorbance of the sample control group.

2.9. In vitro biocompatibility testing of Ber-LPs-PEGDA&PVA MNs

2.9.1. Hemolysis test

Fresh mouse blood was collected and added to an EP tube containing an anticoagulant. The blood cells were separated by centrifuging at 1000 r/min for 15 min. The centrifuged precipitate was washed with PBS until the supernatant was clear and transparent, and the precipitate consisted of blood cells. The final concentration of red blood cells was adjusted to 5 % (v/v) using PBS. Different concentrations of Ber-LPs-PEGDA&PVA MNs were placed in the aforementioned red blood cell solution. PBS and 1 % TritonX-100 were used as negative and positive controls, respectively, with hemolysis rates of 0 % and 100 %. Each group was incubated at 37 °C for 2 h, and photographs were taken after centrifugation. The supernatant from centrifugation was collected, and its absorbance value at 450 nm was measured. The hemolysis rate (%) was calculated using the following formula:

$$\text{Hemolysis rate}\ (\%) = \frac{A_s\text{-}A_n}{A_p\text{-}A_n} \times 100\%$$

where "A_s" represents the absorbance value of the sample group, "A_p" and "A_n" represent the absorbance value of the positive control group and the negative control group.

2.9.2. Cytotoxicity test

A suitable amount of high-glucose DMEM culture medium was added to the Ber-LPs-PEGDA&PVA MNs, which were then filtered across the 0.22 μm syringe filter. After adding 10 % fetal bovine serum and 1 % double antibiotics, MNs extracts of different concentrations (0.04, 0.08, 0.12, 0.16 mg/mL) were obtained. CCK8 assay was employed to evaluate the cell viability of mouse fibroblasts (L929) cocultured with these MNs extracts for 24 and 48 h. The passaged L929 cells were cultured until the cell density reached 80 %–90 % of the entire culture dish. They were then digested with trypsin and seeded into a 96-well plate at a density of 1×10^4 cells per well. After incubating for 24 h to allow cell attachment, different concentrations of MNs extracts were added for incubation. At the predetermined time points, the wells were washed, and CCK8 reagent was added to the samples for incubation for 2 h. Subsequently, a microplate reader was used to measure the cell viability at a wavelength of 450 nm.

2.10. Establishment and treatment of psoriatic mode

After three days of adaptive feeding, the mice were anesthetized and then shaved on their backs to create an area of approximately 2 cm × 2 cm. The shaved area was treated with depilatory cream (Veet, France). The mice were then fed normally for 24 h to allow the stratum corneum (the outermost layer of skin) to recover. Following this, the mice were randomly divided into eight groups, with five mice in each group. Over the next seven days, the psoriasis model was induced by daily application of imiquimod cream (IMQ), followed by drug administration after 8 h. The grouping was as follows: Control group (no treatment received), DEX group (0.1 mg/10g of dexamethasone cream), Model group (0.1 mL of saline applied), Ber group (0.1 mL, 2 mg/mL), Ber-LPs group (0.1 mL, 2 mg/mL), BMNs group (one piece of drug-free microneedle patch), Ber-LPs-PEGDA MNs group (one piece of drug microneedle patch), and Ber-LPs-PEGDA&PVA MNs group (one piece of drug microneedle patch). The body weight of the mice was recorded daily. The dorsal skin of the mice was photographed each day to document the progression of lesions. Scores were assigned based on the Psoriasis Area and Severity Index (PASI score) for erythema, scaling, and thickness, with the following scale: 0 = none, 1 = mild, 2 = moderate, 3 = severe, 4 = very severe. On the seventh day, blood, skin, and major organs were collected from the mice for further analysis.

2.11. Histological analysis and epidermal thickness

To further observe the skin pathological changes in mice with psoriasis, as well as the epidermal thickness and degree of inflammatory cell infiltration, H&E staining was performed on mouse skin sections in this study, followed by histological observation of the changes using a pathological section scanner.

2.12. Immunohistochemical analysis

The immunohistochemical method was used to detect the expression of CD31 and VEGF-related proteins in the skin. Prepared paraffin sections were subjected to dewaxing and hydration, followed by thermal repair with antigen retrieval solution. After blocking, the primary antibody was added and incubated overnight at 4 °C. The sections were then retrieved, and the diluted secondary antibody was added, followed by incubation at 37 °C for 60 min. Freshly prepared diaminobenzidine (DAB) chromogenic solution was also added. When brownish-yellow positive particles appeared in the target tissue and no nonspecific coloration was observed in the surrounding tissues under the microscope, the sections were placed in distilled water to stop the color development. Counterstaining and mounting were then performed. The obtained immunohistochemical sections were placed under a microscope for observation, and 3–5 random fields were selected. The number of positive cells was analyzed using Image J.

2.13. Detection of serum cytokine levels and hepatorenal function

Collect blood samples from mice, let them stand still at room temperature for 2–3 h, centrifuge at 3000 rpm for 20 min, and then remove the serum from the supernatant. Serum levels of TNF-α, IFN-γ, IL-23, IL-17, ALT, AST, UREA, and CREA were measured according to the ELISA kit instructions.

2.14. Detection of oxidative stress-related factors in skin tissue

After homogenizing the mouse skin tissue, the superoxide dismutase (SOD), catalase (CAT), glutathione peroxidase (GSH-Px), and malondialdehyde (MDA) levels in the skin tissue were detected according to the instructions for the measured indicators.

2.15. Statistical analysis

Statistical analysis was performed using GraphPad Prism version 9.0 (GraphPad). All data are presented as mean ± standard deviation (SD). Statistical differences between two groups were analyzed using unpaired Student's t-test, while comparisons among multiple groups were conducted using one-way ANOVA. A p-value <0.05 was considered statistically significant ($^*p < 0.05$, $^{**}p < 0.01$,$^{***}p < 0.001$, $^{****}p < 0.0001$, ns > 0.05.).

3. Results and discussion

3.1. Formulation and characterization of Ber-LPs

To prepare Ber-LPs with high encapsulation efficiency and stable particle size, the main parameters of the Ber-LPs preparation process were optimized using the Box-Behnken design method, with encapsulation efficiency as the evaluation index. Fig. 1E presents the variable response plot for encapsulation efficiency. The response surface analysis plot, a three-dimensional spatial diagram displaying the relationship between the experimental response value and independent variables, can intuitively show the optimal parameters and the interactions between them. The plot reveals that as the variables A (phospholipid concentration), B (ratio of phospholipid-to-cholesterol), and C (ratio of phospholipid-to-drug) increase, the encapsulation efficiency first rises to a maximum and then decreases. The final formula for the encapsulation efficiency model equation, calculated based on the actual factors, is: EE % = −277.86744 + 46.77742 × A + 24.33603 × B + 48.13525 × C - 0.25833 × AB + 1.10750 × AC + 0.53250 × BC - 3.20356 × A^2 - 1.53853 × B^2 - 7.50675 × C^2. Finally, the formulation of Ber-LPs was determined, with the ratio of phospholipid/cholesterol/drug being 7.96:1:1.97. The appearance of the Ber-LPs prepared under these conditions is shown in Fig. 1C. The TEM results of Ber-LPs (Fig. 1B–S1) indicate a particle size of approximately 200 nm, which is consistent with the particle size result from dynamic light scattering (DLS) (Fig. 1C) of 205.13 ± 4.11 nm. The PDI value is 0.114 ± 0.04, and the Zeta potential is −36.4 ± 0.75 mV (Fig. 1D). Liposomes can be considered relatively stable in solution when the absolute value of their Zeta potential exceeds 20 mV [41]. The liposomes obtained in this experiment exhibit a uniform particle size distribution and display a strong negative electrical charge, indicating a high degree of stability in the system.

3.2. Characterization of MNs

In this study, the photopolymerization method was employed to fabricate MNs, with Ber-LP integrated into the MNs (Fig. 2B). Poly (ethylene glycol) diacrylate (PEGDA, molecular weight of 10,000) and polyvinyl alcohol (PVA) were selected as the matrix materials for MNs

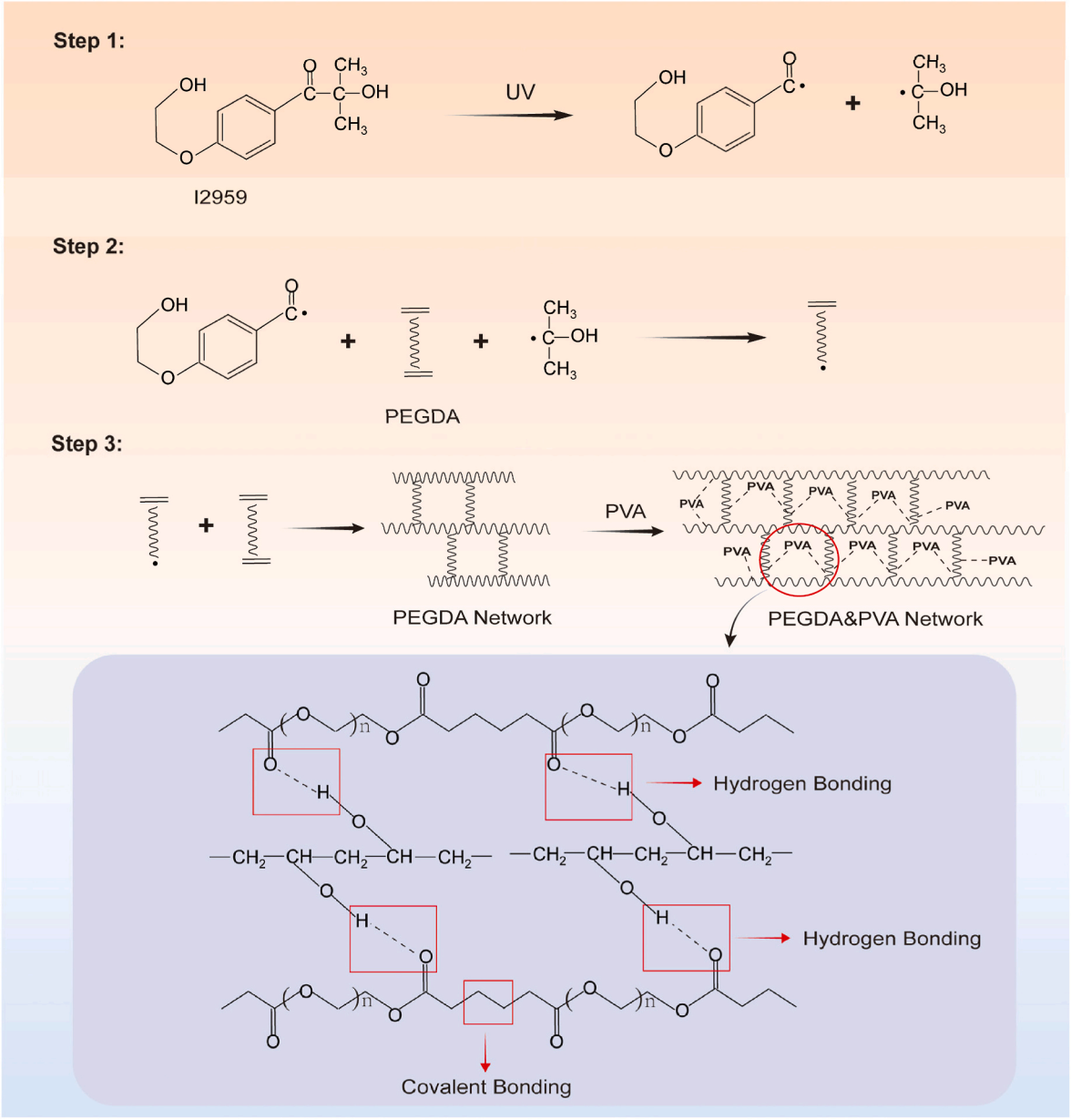

Fig. 3. The formation process of PEGDA&PVA interpenetrating polymer networks.

due to their safety and high biocompatibility. By screening the matrix material ratios (Tables S1 and S2) and considering factors such as the swelling rate, drug release, and structural stability of the MNs, the optimal ratio of PEGDA to PVA was determined to be 10:3.

I2959, as a photoinitiator, undergoes dissociation under UV light to generate radicals. The hydrophilic PEGDA, containing -CH=CH_2 groups at its terminals, reacts with these free radicals to form active centers, which subsequently create a robust network structure through covalent bonds. PVA penetrates into the three-dimensional hydrogel network of PEGDA, forming an interpenetrating polymer network through hydrogen bonding. This increases the cross-linking density of the PEGDA hydrogel network and enables better control over drug release (Fig. 3).

Fourier-transform infrared spectroscopy (FTIR) analysis of the components of PEGDA MNs and PEGDA&PVA MNs (Fig. 2C) revealed that in PEGDA&PVA MNs, the characteristic peaks of -CH=CH_2 groups of PEGDA macromonomers at 810, 1406, and 1635 cm^{-1} became weaker. The strong and broad absorption peak of hydroxyl groups in PVA at 3436 cm^{-1} disappeared in PEGDA&PVA MNs because when PVA cross-links with PEGDA, the hydroxyl groups participate in forming a new hydrogen-bonding network. This hydrogen-bond formation can alter the chemical environment of the hydroxyl groups, thereby affecting their infrared absorption characteristics. Similarly, due to the invariance during the cross-linking process, the ester bond -C=O stretching vibration peak of PEGDA at 1724 cm^{-1} served as an internal reference peak in PEGDA&PVA MNs. The traditional double-bond absorption peak at 1635 cm^{-1} almost completely disappeared, attributed to the successful conversion of carbon-carbon double bonds to carbon-carbon single bonds during the photopolymerization reaction.

The viscoelasticity of the skin can reduce the penetration force of MNs, and MNs must possess sufficient mechanical strength to penetrate the skin. Therefore, the mechanical properties of the MNs were investigated using a texture analyzer (Fig. 2D). The force-displacement curves (Fig. 2E) showed that the maximum force that PEGDA MNs could withstand was 1.08 N, while PEGDA&PVA MNs could withstand a

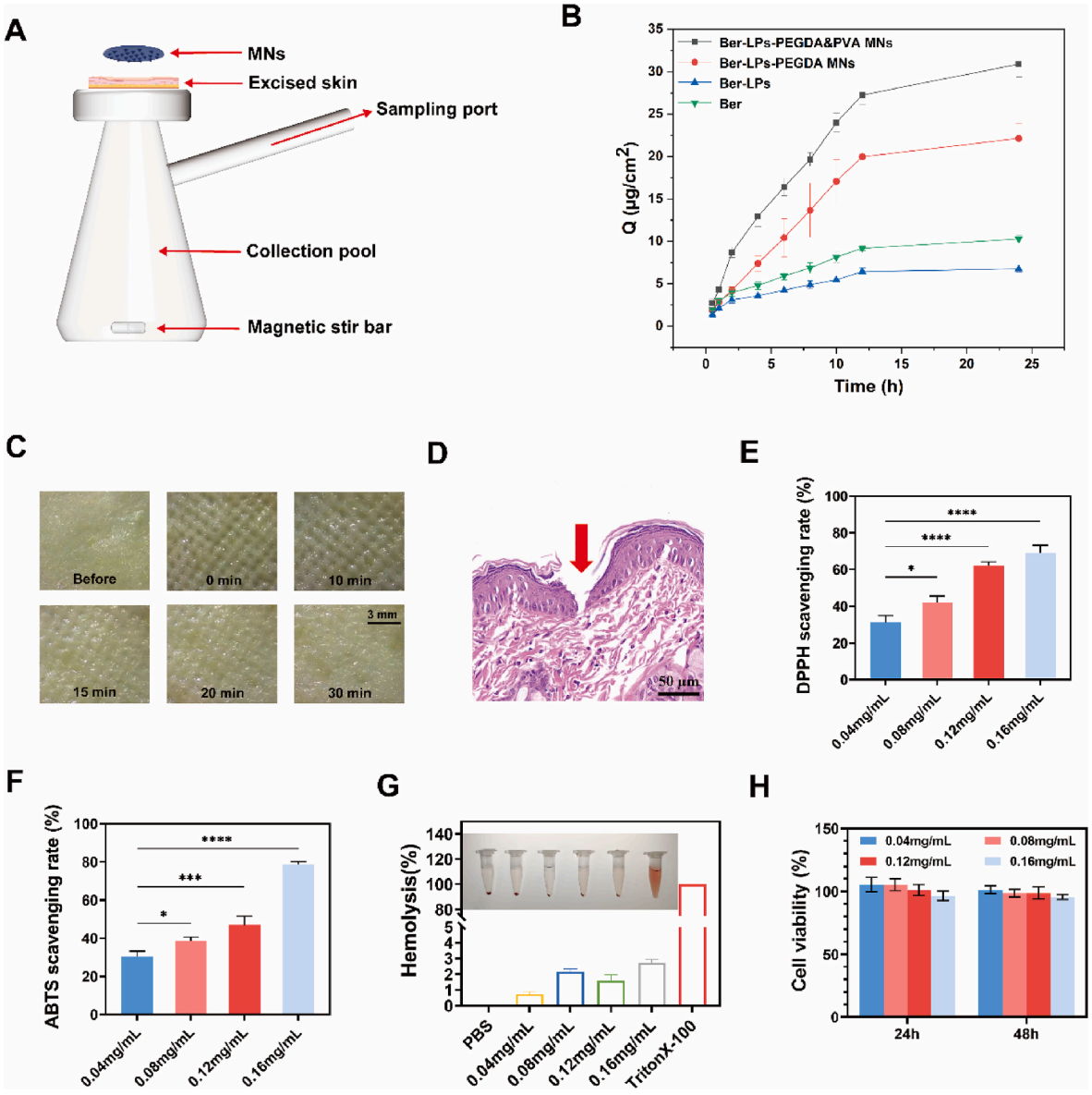

Fig. 4. In vitro experiments of MNs. (A) Franz diffusion cell diagram for transdermal diffusion. (B) Cumulative release curve per unit area (mean ± SD, n = 3). (C) Skin recovery status after application of Ber-LPs-PEGDA&PVA MNs. (D) H&E staining of skin biopsy sections after application of Ber-LPs-PEGDA&PVA MNs. (E) Scavenging rates of DPPH and ABTS (F) by Ber-LPs-PEGDA&PVA MNs at different concentrations. (G) Hemolysis rates of extracts from Ber-LPs-PEGDA&PVA MNs at different concentrations; inset shows images of the hemolysis test. (H) Cell viability of L929 cells after incubation with extracts from Ber-LPs-PEGDA&PVA MNs for 24 h and 48 h at different concentrations. Data are presented as mean ± SD, n = 3, *p < 0.05, ***p < 0.001, ****p < 0.0001, ns > 0.05.

maximum force of 6.20 N. The enhancement in mechanical properties of PEGDA through cross-linking with PVA indicates that the prepared MNs have sufficient mechanical strength to puncture mouse skin.

As shown in Fig. 2F, the prepared MNs exhibit a complete structure and neat arrangement. Widefield THUNDER system images (Fig. 2G) revealed that Ber-LPs were uniformly dispersed in the polymer matrix. SEM images showed that the MNs had a quadrangular pyramid shape with a small and sharp tip and uniform size distribution. The base side length was 280 μm, and the tip height was 450 μm, with a sharp tip facilitating skin insertion. PEGDA&PVA MNs exhibited micron-sized granular structures on their surfaces (Fig. 2H and I), while PEGDA MNs displayed a smoother surface texture and layered structure (Fig. 2J and K), possibly due to the aggregation of PVA molecules in the PEGDA matrix.

3.3. In vitro transdermal release study of MNs

The drug loading of Ber-LPs-PEGDA&PVA MNs was measured to be 186.66 ± 1.47 μg, and that of Ber-LPs-PEGDA MNs was 184.21 ± 0.85 μg. The results of the transdermal experiment (Fig. 4B) showed that compared with Ber and Ber-LPs, Ber-LPs-PEGDA&PVA MNs and Ber-LPs-PEGDA MNs significantly enhanced the transdermal permeability of Ber. Among them, the cumulative release amount per unit area of Ber-LPs-PEGDA&PVA MNs within 24 h was 30.90 ± 1.55 μg/cm^2 and that of Ber-LPs-PEGDA MNs was 22.15 ± 1.76 μg/cm^2. This indicates that the porous structure formed after swelling through cross-linking of PEGDA and PVA is conducive to drug diffusion, while the pure PEGDA network may have limited swelling due to higher cross-linking density, resulting in a slower drug release rate. In contrast, the cumulative release amount per unit area of Ber and Ber-LPs within 24 h was only 10.2 ± 0.43 μg/cm^2 and 6.75 ± 0.37 μg/cm^2, respectively, suggesting that liposomes have a good sustained-release effect on Ber, and microneedles can effectively promote transdermal drug absorption.

3.4. Insertion experiment of Ber-LPs-PEGDA&PVA MNs

As shown in Fig. 4C, after the removal of Ber-LPs-PEGDA&PVA MNs, neatly arranged puncture marks were visible to the naked eye. However, over time, these marks gradually disappeared and were almost undetectable within 30 min. Throughout this process, no significant irritation reactions (such as erythema or swelling) were observed, indicating that Ber-LPs-PEGDA&PVA MNs do not irritate the skin and cause minimal trauma to it, demonstrating good safety. The H&E staining results of the skin sections provided direct evidence of skin tissue puncture at each insertion point of the microneedles (Fig. 4D). The insertion depth of Ber-LPs-PEGDA&PVA MNs into the skin was approximately 150 μm, accounting for 33.3 % of the total needle height. These results indicate that the MNs can effectively penetrate the stratum corneum to reach the dermis and deliver Ber to the superficial skin lesions.

3.5. Antioxidant capacity of Ber-LPs-PEGDA&PVA MNs

Radicals play a crucial role in the exacerbation of inflammation, disruption of the skin barrier, and abnormal cell proliferation in psoriasis through oxidative stress mechanism [42], making the ability of drugs to scavenge radicals of vital importance. In the DPPH (Fig. 4E) and ABTS (Fig. 4F) radical scavenging assays, the scavenging abilities of Ber-LPs-PEGDA&PVA MNs on both DPPH and ABTS radicals increased with their concentration, showing a concentration-dependent relationship. At a concentration of 0.16 mg/mL, Ber-LPs-PEGDA&PVA MNs exhibited maximum scavenging rates of 69.21 ± 4.05 % for DPPH radicals and 78.66 ± 1.54 % for ABTS radicals. These results indicate that Ber-LPs-PEGDA&PVA MNs possess significant radical scavenging capacity and potential to reduce oxidative damage.

3.6. In vitro biocompatibility testing of Ber-LPs-PEGDA&PVA MNs

Good biocompatibility is essential for Ber-LPs-PEGDA&PVA MNs, as they directly contact the wound area of psoriasis. Therefore, we evaluated the blood compatibility and cellular compatibility of different concentrations of Ber-LPs-PEGDA&PVA MNs. The hemolysis test results are shown in Fig. 4G. The suspension of the positive control group exhibited a red color, with no red blood cell precipitates at the bottom of the tube. The suspension of the negative control group was colorless, with red blood cell precipitates at the bottom. Similar to the negative control group, all Ber-LPs-PEGDA&PVA MNs groups showed colorless or lightly colored suspensions, with red blood cell precipitates at the bottom, indicating that no hemolysis occurred, and the hemolysis rates of all groups were below 5 %. This demonstrated their good blood compatibility. The CCK8 test results also showed that after incubation for 24 h and 48 h, the viability of L929 cells in all groups was above 95 % (Fig. 4H), proving the good cellular compatibility of Ber-LPs-PEGDA&PVA MNs.

3.7. In vivo studies on anti-psoriatic effects of Ber-LPs-PEGDA&PVA MNs

To assess the therapeutic potential of Ber-LPs-PEGDA&PVA MNs for treating psoriatic skin inflammation, an IMQ-induced psoriasis-like mouse model and a drug administration procedure were established (Fig. 5A). The IMQ-induced model is one of the most widely used and well-established psoriasis models, with pathological features closely resembling human psoriasis [43]. Dexamethasone cream (Dex) was chosen as the positive control drug due to its high anti-inflammatory efficacy among glucocorticoids, which inhibits the infiltration of inflammatory cells and the release of inflammatory mediators, thereby alleviating symptoms in psoriasis patients [44]. As shown in Fig. 5B, mouse body weight changes were recorded, and erythema, scaling, and epidermal thickening on the dorsal skin were observed throughout the experimental period. During treatment, the model group exhibited a significant decrease in body weight compared to the control group ($p < 0.01$), while no significant changes in body weight were observed in the other groups (Fig. 5D). The dorsal skin of mice in the model group was red and rough, with extensive scaling and a marked increase in skin thickness. The Psoriasis Area and Severity Index (PASI) gradually increased with the duration of modeling (Fig. 5E). The BMNs group did not show any improvement in symptoms such as scaling. Both the Ber and Ber-LPs groups reduced the PASI score, while the Ber-LPs-PEGDA&PVA MNs group significantly alleviated psoriasis-like symptoms in mice, reducing erythema and scaling and restoring smoother skin.

To understand the pathological changes in the skin tissue, H&E staining was performed on the lesion sites on the backs of the mice (Fig. 5C). The control group mice exhibited intact skin morphology with no obvious pathological changes. In contrast, the model group mice showed a marked increase in epidermal thickness at the lesion sites, with hyperkeratosis or parakeratosis of the stratum corneum, acanthosis of the spinous layer, and significant infiltration of inflammatory cells. Compared to the model group, the Ber and Ber-LPs groups reduced hyperkeratosis and epidermal thickness to varying degrees, with the Ber-LPs group showing a more significant improvement in alleviating psoriasis symptoms than the Ber group, indicating that Ber-LPs enhanced the bioavailability of Ber. Furthermore, the therapeutic efficacy of the Ber-LPs-PEGDA&PVA MNs group was significantly better than that of the Ber-LPs group, and the Ber-LPs-PEGDA&PVA MNs group reduced the spinous layer thickness more significantly than the Ber-LPs-PEGDA MNs group (Fig. 5F; $p < 0.001$).

The spleen is a vital immune organ in the human body, acting as a reservoir for immune cells and a site for immune responses. Therefore, the spleen index, defined as the ratio of spleen weight to body weight, can serve as a preliminary indicator to assess the inhibitory effects of drugs on immune organs. We compared the spleen indices among

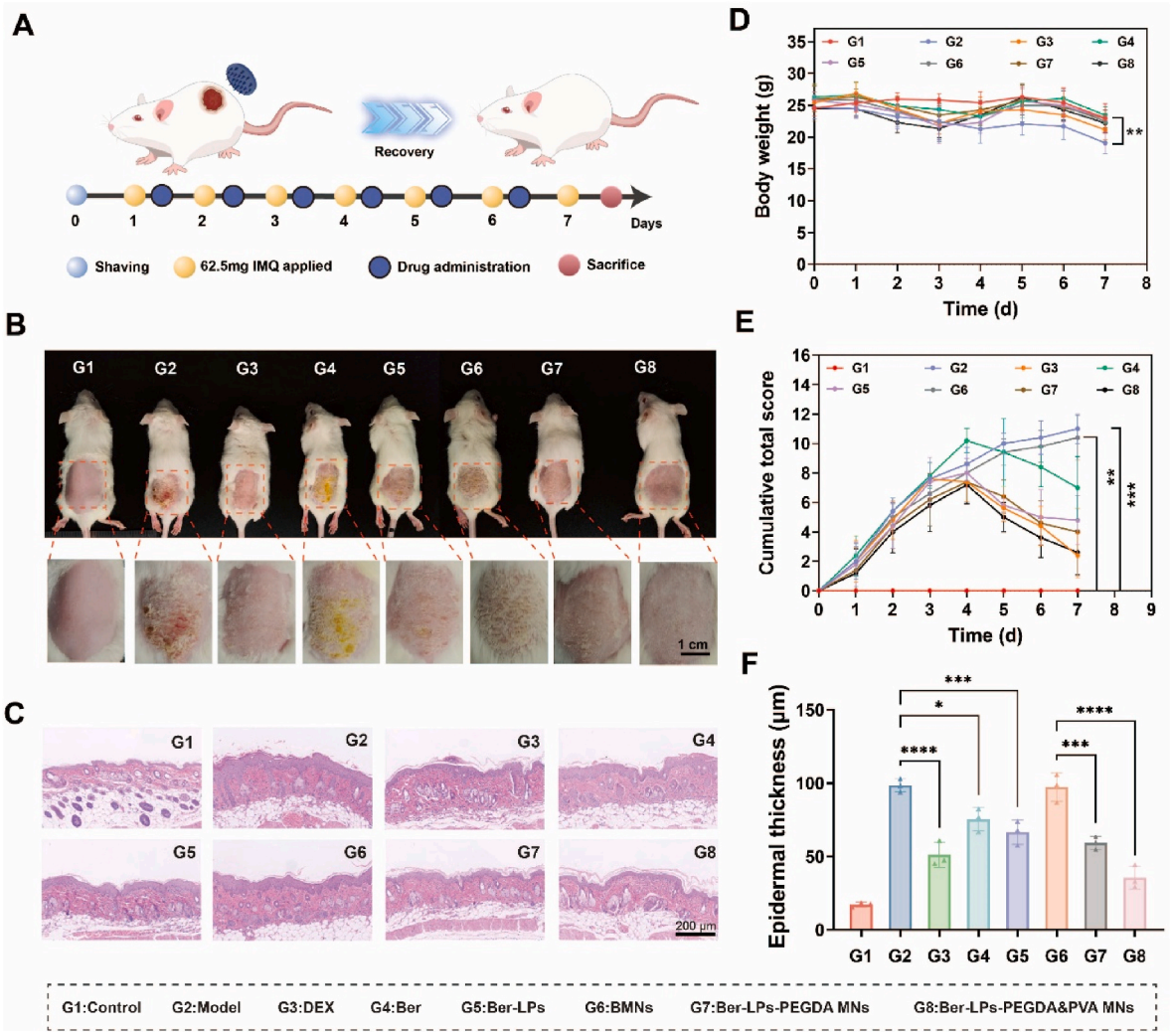

Fig. 5. Therapeutic effects of different groups on psoriasis models. (A) Schematic diagram of the establishment and treatment of the IMQ-induced psoriasis model. (B) Photographs of the dorsal skin of mice treated with different groups. (C) H&E staining of mouse skin sections. (D) Changes in body weight during treatment. (E) Epidermal thickness of the skin measured from skin sections. Data are presented as mean ± SD (n = 5), with *p < 0.05, **p < 0.01, ***p < 0.001, and ****p < 0.0001 indicating statistical significance.

different groups. The results showed that the spleen index in the DEX group was the smallest (Fig. 6A and B), likely due to the potent immune suppressive effects of glucocorticoids. The spleen index of mice in the Ber-LPs-PEGDA&PVA MNs group was close to that of the control group and significantly lower than that of the model group and the BMNs group. This indicates a certain degree of immune suppression without reducing the spleen index.

During the pathogenesis of psoriasis, the most significant pathological changes are the excessive proliferation of keratinocytes and the proliferation of blood vessels in the superficial dermis. When keratinocytes are stimulated, they secrete large amounts of VEGF. This induces the proliferation and migration of endothelial cells, stimulates neovascularization, and enhances the sensitivity of vascular endothelial cells to VEGF, accelerating neovascularization and promoting the occurrence and progression of psoriasis [45]. CD31, also known as platelet-endothelial cell adhesion molecule (PECAM-1), is widely expressed on the surface of vascular endothelial cells and serves as an important marker for neovascularization [46]. We performed immunohistochemical staining to detect the expression of VEGF and CD31 proteins (Fig. 6E). The results showed that the expression levels of VEGF and CD31 proteins were significantly higher in the model group and BMNs group compared to the control group (Fig. 6C and D, $p < 0.05$). Compared to the model group, the expression levels of CD31 and VEGF proteins were significantly reduced in all drug-treated groups. Among them, the Ber-LPs-PEGDA&PVA MNs group exhibited the most significant reduction in CD31 and VEGF protein expression ($p < 0.001$). This indicates that combining MNs with liposomes can help drugs penetrate the thickened epidermis, enhance drug retention in the skin, and achieve the therapeutic goal of treating psoriasis.

The precise pathogenesis of psoriasis is still not fully understood. However, it is thought that the IL-23/Th17 axis may work together with the IFN-γ/TNF-Th1 axis, both contributing to the development of psoriasis. IL-23 from dendritic cells (DC) directly stimulates Th17 cells, causing them to produce lots of inflammatory cytokines like IL-17A and IL-17F. These cytokines directly affect keratinocytes (KC) [47]. In response, KC produce VEGF, leading to changes in psoriatic skin such as thicker epidermis, parakeratosis, and new blood vessel growth. IL-23 from KC can further activate Th17 cells. Meanwhile, IL-12 from activated DC directly stimulates Th1 cells to produce plenty of TNF-α and IFN-γ. TNF-α makes fibroblasts release keratinocyte growth factor (KGF), which helps KC grow more [48]. These inflammatory cytokines work together in a network, pushing psoriasis to get worse [49]. ELISA kits were used to check the levels of TNF-α, IFN-γ, IL-23, and IL-17 in the serum of each group. The skin lesions were analyzed based on these cytokine levels. The results (Fig. 6F) showed that the model group and the BMNs group had much higher levels of TNF-α, IFN-γ, IL-23, and

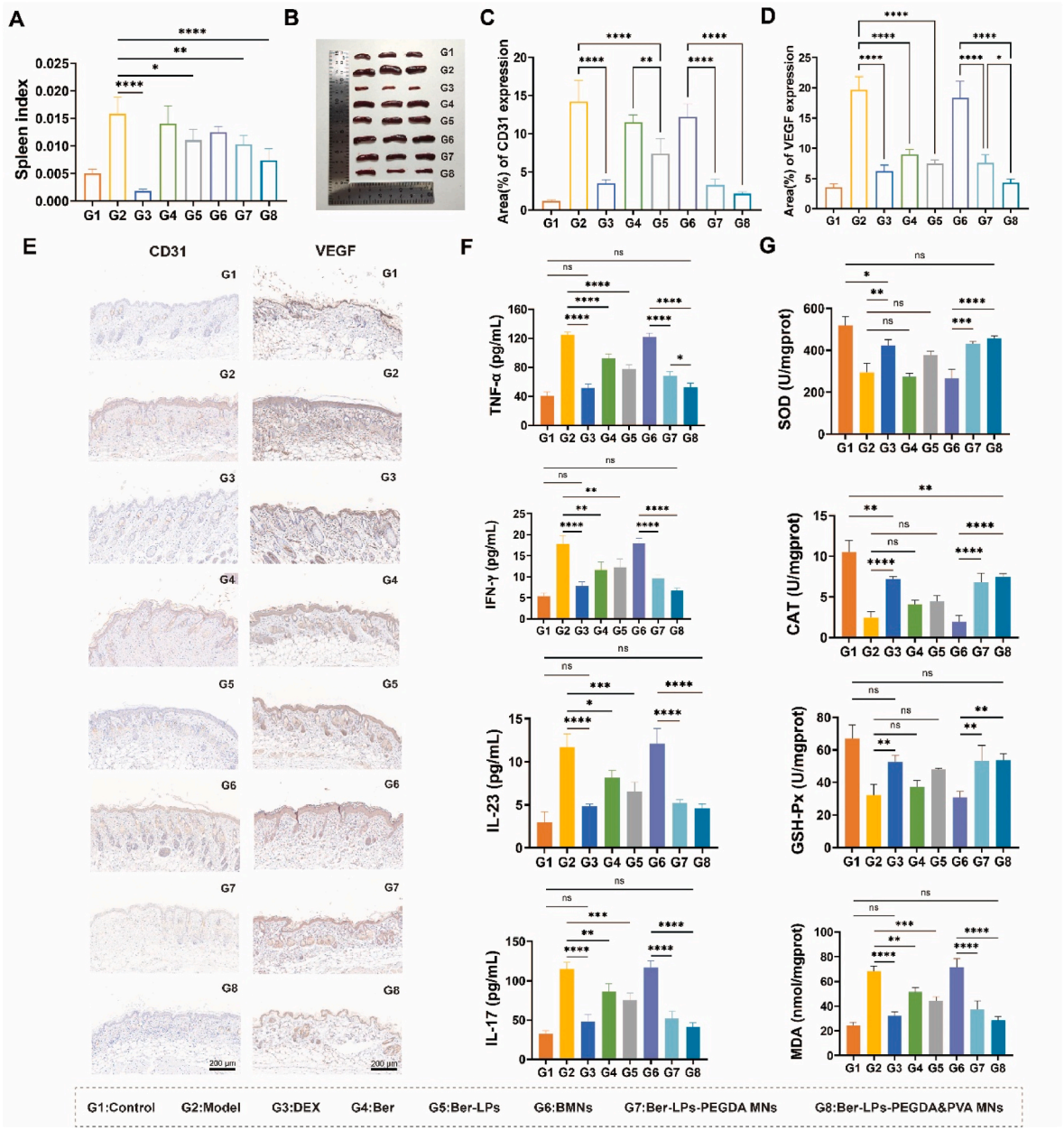

Fig. 6. Therapeutic effects of different groups on psoriasis models. (A) Spleen index. (B) Digital images of the spleen. (C) Positive expression rate of CD31 in mouse skin sections. (D) Positive expression rate of VEGF in mouse skin sections. (E) Immunohistochemical micrographs of CD31 and VEGF in mouse skin sections. (F) Expression levels of IFN-γ, TNF-α, IL-17, and IL-23 in the serum of psoriasis mice from different formulation groups. (G) Expression levels of CAT, GSH-Px, MDA, and SOD in the skin tissues of psoriasis mice from different formulation groups. Data are presented as mean ± SD (n = 5), Data are presented as mean ± SD, n = 3, *p < 0.05, **p < 0.01, ***p < 0.001, ****p < 0.0001, ns > 0.05.

IL-17 in their serum compared to the control group ($p < 0.0001$). In contrast, the DEX group and the MNs group had similar levels of these cytokines to the control group ($p > 0.05$). Compared to the model group, all drug treatments lowered the levels of these cytokines ($p < 0.05$), with the MNs group having a stronger effect than the Ber group and the Ber-LPs group ($p < 0.01$). This suggests that Ber-LPs-PEGDA&PVA MNs can somewhat stop this kind of inflammation from happening. In addition, liver and kidney function tests were conducted on the mice in each group. No significant differences were observed in serum ALT, AST, urea, and CREA levels between the treatment group and the normal group (Fig. S2). These results indicate that MNs within the dosage range studied have little to no impact on the liver and kidney functions of mice.

Psoriasis mainly shows up because keratinocytes (KC) are not working properly, causing more reactive oxygen species (ROS) in these cells [50]. ROS are made by the immune system and can protect the body, but when there are too many ROS, more genes in inflammatory cells get turned on, making the inflammation worse [51,52]. Superoxide dismutase (SOD), catalase (CAT), and glutathione peroxidase (GSH-Px) are important enzymes in the body that clean up ROS and fight oxidative stress [50]. Malondialdehyde (MDA), which comes from lipid peroxidation, shows how strong the free radical attack on the body is. So, these four things (SOD, CAT, GSH-Px, and MDA) can tell us about oxidative stress damage in the body. The results (Fig. 6G) showed that the model group had much lower levels of SOD, CAT, and GSH-Px in their skin tissue, but higher levels of MDA compared to the control group. This means the model group had weaker antioxidant ability and more oxidative stress damage. The MNs group had similar levels of these four

indicators to the control group ($p > 0.05$), suggesting they could improve the oxidative stress damage caused by IMQ. Compared to the model group, both the Ber group and the Ber-LPs group had some antioxidant ability. However, the Ber-LPs-PEGDA&PVA MNs were even better at balancing the antioxidant enzymes and oxidative intermediates.

In summary, encapsulating drugs into liposomes can enhance the solubility and bioavailability of Ber. In the psoriasis model, the thickened epidermis makes it difficult for Ber-LPs alone to penetrate the skin. However, microneedles loaded with Ber-LPs can deliver the liposomes into the thickened epidermis of psoriasis, avoiding biological barriers such as the stratum corneum obstruction, first-pass effect, and clearance by blood circulation. Additionally, microneedles prepared by cross-linking PVA and PEGDA exhibit a higher degree of cross-linking and swelling ratio compared to those made solely of PEGDA, allowing for better control of the release rate of berberine-loaded liposomes in vivo. Relying solely on PEGDA may lead to rapid drug release, with local drug concentrations peaking and then quickly declining, making it difficult to maintain a long-term inhibitory effect. The addition of PVA, by modulating the polymer ratio, may balance the release rate, avoid burst release, and prolong the duration of drug action. PEGDA dominates the initial rapid release, while PVA controls the sustained release in the later stages, thus covering a longer therapeutic window. In summary, Ber-LPs-PEGDA&PVA MNs hold great promise and provide strong experimental evidence for further development of drug delivery systems based on microneedle technology.

4. Conclusions

In this study, we successfully developed a novel drug delivery system for the treatment of psoriasis: Berberine Hydrochloride-Loaded Liposomes-in-Hydrogel Microneedles (Ber-LPs-PEGDA&PVA MNs). By optimizing the preparation process of the liposomes, we obtained Ber-LPs with high encapsulation efficiency and stable particle size. These were then combined with PEGDA and PVA to fabricate microneedles with good morphology, mechanical strength, and drug release behavior. In vitro experiments demonstrated that the microneedles possess good antioxidant capacity and biocompatibility, without causing significant skin irritation or immune reactions. Furthermore, in vivo experiments confirmed that Ber-LPs-PEGDA&PVA MNs significantly improved symptoms in an imiquimod-induced psoriasis mouse model, reducing the thickness of the spinous layer, alleviating the infiltration of inflammatory cells, decreasing the levels of inflammatory cytokines such as TNF-α, IFN-γ, IL-23, and IL-17, and reducing the expression of angiogenesis-related proteins, thus showing good therapeutic effects. In summary, the Ber-LPs-PEGDA&PVA MNs prepared in this study hold great potential for the treatment of psoriasis and can be extended for the treatment of other complex skin diseases.

CRediT authorship contribution statement

Si Shen: Writing – original draft, Methodology, Investigation, Formal analysis, Data curation. **Wang Shen:** Writing – original draft, Methodology, Investigation, Formal analysis, Data curation. **Lu Wang:** Writing – original draft, Methodology, Investigation, Formal analysis, Data curation. **Bin Sun:** Resources, Investigation, Formal analysis. **Yongli Zhang:** Resources, Investigation, Formal analysis. **Yong Zhang:** Resources, Investigation, Formal analysis. **Ruoyang Jia:** Software, Investigation, Formal analysis. **Yang Wu:** Software, Investigation, Formal analysis. **Xue Chen:** Resources, Formal analysis, Data curation. **Keang Cao:** Software, Investigation, Formal analysis. **Yuqing Fang:** Resources, Formal analysis, Data curation. **Hongmei Xia:** Writing – review & editing, Supervision, Project administration, Funding acquisition, Conceptualization.

Declaration of competing interest

The authors declare no conflict of interest.

Acknowledgments

This study was supported by the Anhui Provincial Quality Engineering Project for Education in the New Era-Research on the Reform of Graduate Education and Teaching (2023jyjxggyjY168), the Department of Education of Anhui Province of China (KJ2019A0470 and 2023AH050754), the Quality Engineering Project of the Anhui Provincial Department of Education in 2021 (2021jyxm0824), the Research and Development Project Entrusted by the Enterprise: Research on the Antioxidant Biological Activity of Quercetin (2022HZ049), the Natural Science Foundation of Anhui Province of China (1608085MH227), and the Quality Engineering Project of Anhui University of Chinese Medicine in 2021 (2021zlgc042).

Appendix A. Supplementary data

Supplementary data to this article can be found online at https://doi.org/10.1016/j.mtbio.2025.101795.

Data availability

Data will be made available on request.

References

[1] C.E.M. Griffiths, A.W. Armstrong, J.E. Gudjonsson, J. Barker, Psoriasis, Lancet 397 (10281) (2021) 1301–1315.
[2] M.A. Lowes, M. Suarez-Farinas, J.G. Krueger, Immunology of psoriasis, Annu. Rev. Immunol. 32 (2014) 227–255.
[3] M. Perry, Psoriasis: an overview, Br. J. Nurs. 33 (15) (2024) 686–692.
[4] A. Luengas-Martinez, R. Paus, H.S. Young, Antivascular endothelial growth factor-A therapy: a novel personalized treatment approach for psoriasis, Br. J. Dermatol. 186 (5) (2022) 782–791.
[5] V. Sobolev, M. Muminova, O. Zhukova, E. Denisova, A. Soboleva, N. Potekaev, I. Korsunskaya, A. Mezentsev, HGF, HNRPD, and sFLT1 interfere with the induction of VEGF in patients with severe psoriasis, Curr. Mol. Med. 24 (2024).
[6] D.E. Branisteanu, C. Cojocaru, R. Diaconu, E.A. Porumb, A.I. Alexa, A.C. Nicolescu, I. Brihan, C.M. Bogdanici, G. Branisteanu, A. Dimitriu, M. Zemba, N. Anton, M. P. Toader, A. Grechin, D.C. Branisteanu, Update on the etiopathogenesis of psoriasis, Exp. Ther. Med. 23 (3) (2022) 201 (Review).
[7] Y. Qu, D. Li, H. Xiong, D. Shi, Transcriptional regulation on effector T cells in the pathogenesis of psoriasis, Eur. J. Med. Res. 28 (1) (2023) 182.
[8] S. Chhabra, S. Dogra, K. Sharma, S.K. Raychaudhuri, S.P. Raychaudhuri, Recent update on immunopathogenesis of psoriasis, Indian J. Dermatol. 67 (4) (2022) 360–373.
[9] G. Balakirski, S. Gerdes, S. Beissert, F. Ochsendorf, R. von Kiedrowski, D. Wilsmann-Theis, Psoriasis-Therapie wahrend Schwangerschaft und Stillzeit, J Dtsch Dermatol Ges 20 (5) (2022) 653–685.
[10] K. Yadav, A. Soni, D. Singh, M.R. Singh, Polymers in topical delivery of anti-psoriatic medications and other topical agents in overcoming the barriers of conventional treatment strategies, Prog. Biomater. 10 (1) (2021) 1–17.
[11] U.U. Mohd Nordin, N. Ahmad, N. Salim, N.S. Mohd Yusof, Lipid-based nanoparticles for psoriasis treatment: a review on conventional treatments, recent works, and future prospects, RSC Adv. 11 (46) (2021) 29080–29101.
[12] Y. Wang, G. Jiang, Advances in the novel nanotechnology for targeted tumor therapy by transdermal drug delivery, Anti Cancer Agents Med. Chem. 22 (15) (2022) 2708–2714.
[13] A. Golubovic, S. Tsai, B. Li, Bioinspired lipid nanocarriers for RNA delivery, ACS Bio Med Chem Au 3 (2) (2023) 114–136.
[14] L. Pourtalebi Jahromi, M. Rothammer, G. Fuhrmann, Polysaccharide hydrogel platforms as suitable carriers of liposomes and extracellular vesicles for dermal applications, Adv. Drug Deliv. Rev. 200 (2023) 115028.
[15] E.D. Castaneda-Reyes, M.J. Perea-Flores, G. Davila-Ortiz, Y. Lee, E. Gonzalez de Mejia, Development, characterization and use of liposomes as amphipathic transporters of bioactive compounds for melanoma treatment and reduction of skin inflammation: a review, Int. J. Nanomed. 15 (2020) 7627–7650.
[16] Y. Zhang, S. Gong, L. Liu, H. Shen, E. Liu, L. Pan, N. Gao, R. Chen, Y. Huang, Cyclodextrin-coordinated liposome-in-gel for transcutaneous Quercetin delivery for psoriasis treatment, ACS Appl. Mater. Interfaces 15 (34) (2023) 40228–40240.
[17] Y. Cui, Q. Zhou, M. Jin, S. Jiang, P. Shang, X. Dong, L. Li, Research progress on pharmacological effects and bioavailability of berberine, Naunyn-Schmiedebergs Arch Pharmacol 397 (11) (2024) 8485–8514.

[18] H. Cheng, J. Liu, Y. Tan, W. Feng, C. Peng, Interactions between gut microbiota and berberine, a necessary procedure to understand the mechanisms of berberine, J Pharm Anal 12 (4) (2022) 541–555.
[19] M. Hashemzaei, R. Rezaee, A review on pain-relieving activity of berberine, Phytother Res. 35 (6) (2021) 2846–2853.
[20] Z. Qin, R. Tang, J. Liang, X. Jia, Berberine, a natural alkaloid: advances in its pharmacological effects and mechanisms in the treatment of autoimmune diseases, Int. Immunopharmacol. 137 (2024) 112422.
[21] F. Shakeri, S. Kiani, G. Rahimi, M.H. Boskabady, Anti-inflammatory, antioxidant, and immunomodulatory effects of Berberis vulgaris and its constituent berberine, experimental and clinical, a review, Phytother Res. 38 (4) (2024) 1882–1902.
[22] J.W. Noh, M.S. Jun, H.K. Yang, B.C. Lee, Cellular and molecular mechanisms and effects of berberine on obesity-induced inflammation, Biomedicines 10 (7) (2022).
[23] K.K. Mishra, C.D. Kaur, S. Singh, A. Tiwari, V. Tiwari, A. Sharma, Assessing the efficacy of berberine hydrochloride-loaded transethosomal gel system in treating dermatophytosis caused by trichophyton rubrum in ex-vivo, in-vitro and in-vivo models, Curr Drug Res Rev 16 (3) (2024) 412–422.
[24] A. Calvo, E. Moreno, I. Aldalur, C. Sanmartin, E. Larrea, E. Gonzalez-Penas, J. M. Irache, S. Espuelas, Effect of topical berberine in murine cutaneous leishmaniasis lesions, J. Antimicrob. Chemother. 77 (4) (2022) 1072–1081.
[25] Z. Asemi, M. Behnam, M.A. Pourattar, H. Mirzaei, Z.S. Razavi, O.R. Tamtaji, Therapeutic potential of berberine in the treatment of glioma: insights into its regulatory mechanisms, Cell. Mol. Neurobiol. 41 (6) (2021) 1195–1201.
[26] Q. Yang, T. Zhang, Y. Wu, Q. Liang, W. Zhao, R. Liu, X. Jin, Progress in the application of microneedles in eye disorders and the proposal of the upgraded microneedle with spinule, Pharm. Res. 41 (2) (2024) 203–222.
[27] Z. Gao, T. Sheng, W. Zhang, H. Feng, J. Yu, Z. Gu, Y. Zhang, Microneedle-mediated cell therapy, Adv. Sci. (Weinh.) 11 (8) (2024) e2304124.
[28] B. Zheng, Q. Li, L. Fang, X. Cai, Y. Liu, Y. Duo, B. Li, Z. Wu, B. Shen, Y. Bai, S. X. Cheng, X. Zhang, Microorganism microneedle micro-engine depth drug delivery, Nat. Commun. 15 (1) (2024) 8947.
[29] X. Hou, J. Li, Y. Hong, H. Ruan, M. Long, N. Feng, Y. Zhang, Advances and prospects for hydrogel-forming microneedles in transdermal drug delivery, Biomedicines 11 (8) (2023).
[30] J.Y. Li, Y.H. Feng, Y.T. He, L.F. Hu, L. Liang, Z.Q. Zhao, B.Z. Chen, X.D. Guo, Thermosensitive hydrogel microneedles for controlled transdermal drug delivery, Acta Biomater. 153 (2022) 308–319.
[31] X. Gu, Z. Wu, D. Wu, B. Hou, L. Bian, T. Zhou, Y. Hou, H. Wang, Z. Zheng, Hydrogel microneedle patch for treatment of liver fibrosis, Mater. Today Adv. 20 (2023).
[32] L. Yang, Y. Gao, Q. Liu, W. Li, Z. Li, D. Zhang, R. Xie, Y. Zheng, H. Chen, X. Zeng, A bacterial responsive microneedle dressing with hydrogel backing layer for chronic wound treatment, Small 20 (12) (2024) e2307104.
[33] M. Ji, F. Zhan, X. Qiu, H. Liu, X. Liu, P. Bu, B. Zhou, M. Serda, Q. Feng, Research progress of hydrogel microneedles in wound management, ACS Biomater. Sci. Eng. 10 (8) (2024) 4771–4790.
[34] X. Hong, Z. Wu, L. Chen, F. Wu, L. Wei, W. Yuan, Hydrogel microneedle arrays for transdermal drug delivery, Nano-Micro Lett. 6 (3) (2014).
[35] L. Barnum, J. Quint, H. Derakhshandeh, M. Samandari, F. Aghabaglou, A. Farzin, L. Abbasi, S. Bencherif, A. Memic, P. Mostafalu, A. Tamayol, 3D-Printed hydrogel-filled microneedle arrays, Adv. Healthcare Mater. 10 (13) (2021) e2001922.
[36] C. Sebaaly, H. Greige-Gerges, S. Stainmesse, H. Fessi, C. Charcosset, Effect of composition, hydrogenation of phospholipids and lyophilization on the characteristics of eugenol-loaded liposomes prepared by ethanol injection method, Food Biosci. 15 (2016) 1–10.
[37] J. Treml, K. Smejkal, Flavonoids as potent scavengers of hydroxyl radicals, Compr. Rev. Food Sci. Food Saf. 15 (4) (2016) 720–738.
[38] Z. Cheng, Y. Zhang, H. Song, H. Zhou, F. Zhong, H. Hu, Y. Feng, Extraction optimization, characterization and antioxidant activity of polysaccharide from Gentiana scabra bge, Int. J. Biol. Macromol. 93 (Pt A) (2016) 369–380.
[39] E. Alinkina, E. Don, O. Gizitdinova, L. Samsonova, A. Petrova, G. Stepanov, S. Tarasov, A novel technique for studying the effects of technologically processed antibodies by evaluating the rate of oxidation of ascorbic acid during the reduction of the green-blue ABTS + radical, Spectrochim. Acta Mol. Biomol. Spectrosc. 304 (2024) 123323.
[40] Y.-L. Ma, D.-Y. Zhu, K. Thakur, C.-H. Wang, H. Wang, Y.-F. Ren, J.-G. Zhang, Z.-J. Wei, Antioxidant and antibacterial evaluation of polysaccharides sequentially extracted from onion (Allium cepa L.), Int. J. Biol. Macromol. 111 (2018) 92–101.
[41] F. Qu, Y. Sun, D. Bi, S. Peng, M. Li, H. Liu, L. Zhang, J. Tao, Y. Liu, J. Zhu, Regulating size and charge of liposomes in microneedles to enhance intracellular drug delivery efficiency in skin for psoriasis therapy, Adv. Healthcare Mater. 12 (31) (2023) e2302314.
[42] E.C. Dobrica, M.A. Cozma, M.A. Gaman, V.M. Voiculescu, A.M. Gaman, The involvement of oxidative stress in psoriasis: a systematic review, Antioxidants 11 (2) (2022).
[43] J. Song, J. Jiang, L. Kuai, Y. Luo, M. Xing, Y. Luo, Y. Ru, X. Sun, H. Zhang, T. Liu, X. Li, B. Li, TMT-based proteomics analysis reveals the protective effect of Jueyin granules on imiquimod-induced psoriasis mouse model by causing autophagy, Phytomedicine 96 (2022) 153846.
[44] X. Liu, Z. Chen, J. Bai, X. Li, X. Chen, Z. Li, H. Pan, S. Li, Q. Gao, N. Zhao, A. Chen, H. Xu, Y. Wen, L. Du, M. Yang, X. Zhou, J. Huang, Multifunctional hydrogel eye drops for synergistic treatment of ocular inflammatory disease, ACS Nano 17 (24) (2023) 25377–25390.
[45] H.J. Lee, Y.J. Hong, M. Kim, Angiogenesis in chronic inflammatory skin disorders, Int. J. Mol. Sci. 22 (21) (2021).
[46] G. Caligiuri, CD31 as a therapeutic target in atherosclerosis, Circ. Res. 126 (9) (2020) 1178–1189.
[47] X. Wang, S. Feng, N. Ding, Y. He, C. Li, M. Li, X. Ding, H. Ding, J. Li, J. Wu, Y. Li, J. Xu, Anti-inflammatory effects of berberine hydrochloride in an LPS-induced murine model of mastitis, Evid. base Compl. Alternative Med. 2018 (1) (2018).
[48] C. Li, Y. Xi, S. Li, Q. Zhao, W. Cheng, Z. Wang, J. Zhong, X. Niu, G. Chen, Berberine ameliorates TNBS induced colitis by inhibiting inflammatory responses and Th1/Th17 differentiation, Mol. Immunol. 67 (2 Pt B) (2015) 444–454.
[49] M. Zhang, N. Li, R. Cai, J. Gu, F. Xie, H. Wei, C. Lu, D. Wu, Rosmarinic acid protects mice from imiquimod induced psoriasis-like skin lesions by inhibiting the IL-23/Th17 axis via regulating Jak2/Stat3 signaling pathway, Phytother Res. 35 (8) (2021) 4526–4537.
[50] S.P. Cannavo, G. Riso, M. Casciaro, E. Di Salvo, S. Gangemi, Oxidative stress involvement in psoriasis: a systematic review, Free Radic. Res. 53 (8) (2019) 829–840.
[51] L. Wang, C. Wang, C. Huang, C. Gao, B. Wang, J. He, Y. Yan, Dietary berberine against intestinal oxidative stress, inflammation response, and microbiota disturbance caused by chronic copper exposure in freshwater grouper (Acrossocheilus fasciatus), Fish Shellfish Immunol. 139 (2023) 108910.
[52] Z. Pu, H. Wen, H. Jiang, Q. Hou, H. Yan, Berberine improves negative symptoms and cognitive function in patients with chronic schizophrenia via anti-inflammatory effect: a randomized clinical trial, Chin. Med. 18 (1) (2023) 41.